

Continual Reinforcement Learning for Digital Twin Synchronization Optimization

Haonan Tong, *Student Member, IEEE*, Mingzhe Chen, *Member, IEEE*, Jun Zhao, *Member, IEEE*,
Ye Hu, *Member, IEEE*, Zhaohui Yang, *Member, IEEE*, Yuchen Liu, *Member, IEEE*,
Changchuan Yin, *Senior Member, IEEE*

Abstract—This article investigates the adaptive resource allocation scheme for digital twin (DT) synchronization optimization over dynamic wireless networks. In our considered model, a base station (BS) continuously collects factory physical object state data from wireless devices to build a real-time virtual DT system for factory event analysis. Due to continuous data transmission, maintaining DT synchronization must use extensive wireless resources. To address this issue, a subset of devices is selected to transmit their sensing data, and resource block (RB) allocation is optimized. This problem is formulated as a constrained Markov process (CMDP) problem that minimizes the long-term mismatch between the physical and virtual systems. To solve this CMDP, we first transform the problem into a dual problem that refines RB constraint impacts on device scheduling strategies. We then propose a continual reinforcement learning (CRL) algorithm to solve the dual problem. The CRL algorithm learns a stable policy across historical experiences for quick adaptation to dynamics in physical states and network capacity. Simulation results show that the CRL can adapt quickly to network capacity changes and reduce normalized root mean square error (NRMSE) between physical and virtual states by up to 55.2%, using the same RB number as traditional methods.

Index Terms—Digital twin, constrained Markov decision process, continual reinforcement learning.

I. INTRODUCTION

Future wireless networks must support interactive applications such as digital twins (DTs) [1] and Metaverse [2]. These applications necessitate the mapping of a physical system into a synchronized virtual system, facilitated by ubiquitous and continuous sensing data transmission [3], [4]. However,

achieving continuous synchronization between a physical system and its corresponding virtual counterpart faces several challenges. First, the mapping from the physical system to a virtual system requires extensive sensing data transmission, which may be hard to achieve in a wireless network with constrained communication resources [5], [6]. Second, since the data required for the mapping is transmitted over wireless channels, the dynamics (i.e., channel conditions) of wireless environment will significantly affect synchronization between the virtual system and physical system [7], [8].

A. Related Works

Recently, several works such as [9]–[16] have studied the applications of DT for wireless networks with limited resources. The work in [9] developed DT empowered network framework to optimize computational power, storage resource, and communication resource allocation. The authors in [10]–[12] used DT to capture the computational capability of each device to improve federated learning performance under communication and computation resource constraints. In [13], the authors used DT to predict task requirements and network topology so as to reduce task offloading latency and network congestion. The work in [14] used DT to simulate the dynamic bandwidth budget, packet arrival, and throughputs of a network and use this information to improve the spectrum efficiency. The work in [15] utilized DT to simulate the competition for communication and computing resources among multiple devices, where device state estimation errors were corrected by DT, thereby enhancing the performance of the network resource management strategy. Furthermore, in [16], DT was introduced to capture the high mobility of aerial communication nodes, enabling network behavior analysis in non-terrestrial networks. However, most of these works in [9]–[16] that focused on DT applications did not consider how limited wireless resources (i.e., transmit power and spectrum) affect the DT synchronization, which requires continuous data transmission.

The works in [17]–[21] have studied efficient communication mechanisms to optimize DT synchronization. The work in [17] developed a joint communication and computation framework for DT synchronization to reduce communication latency under DT model accuracy constraints. In [18], the authors proposed a hierarchical data collection framework in multi-layer networks to optimize DT synchronization with limited spectrum resources. The work in [19] analyzed the impacts of communication delay on the DT model accuracy.

H. Tong is with the Beijing Key Laboratory of Network System Architecture and Convergence, the Beijing Advanced Information Network Laboratory, Beijing University of Posts and Telecommunications, Beijing, China, and also with the College of Computing and Data Science at Nanyang Technological University (NTU), Singapore. Email: hntong@bupt.edu.cn.

M. Chen is with the Department of Electrical and Computer Engineering and Frost Institute for Data Science and Computing, University of Miami, Coral Gables, FL, 33146, USA, Email: mingzhe.chen@miami.edu.

J. Zhao is with the College of Computing and Data Science at Nanyang Technological University (NTU), Singapore. Email: junzhao@ntu.edu.sg.

Y. Hu is with the Department of Industrial and Systems Engineering, University of Miami, Coral Gables, FL, 33146, USA, Email: yehu@miami.edu.

Z. Yang is with the College of Information Science and Electronic Engineering, Zhejiang University, Hangzhou, Zhejiang 310027, China, Email: yang_zhaohui@zju.edu.cn.

Y. Liu is with the Department of Computer Science, North Carolina State University, Raleigh, NC, 27695, USA, Email: yuchen.liu@ncsu.edu.

C. Yin is with the Beijing Key Laboratory of Network System Architecture and Convergence, and also with the Beijing Advanced Information Network Laboratory, Beijing University of Posts and Telecommunications, Beijing, 100876 China. Email: ccyin@bupt.edu.cn.

In [20], the authors adjusted the device schedule, transmit power, and computing frequency to optimize DT synchronization in unmanned aerial vehicle (UAV)-assisted edge computing networks. The authors in [21] proposed a game theory based network access algorithm to efficiently synchronize the data between the DT and the vehicle. However, most of the works in [17]–[21] assumed that physical objects change according to predetermined probabilities. Due to the dynamic nature of the physical system, the sensing data for building DT actually changes with unpredictable randomness, which is difficult to be modeled. Hence, the sensing data transmission methods for DT synchronization must be adaptive to the changes of the physical system dynamics.

The works in [22]–[28] have studied adaptive network resource management methods to guarantee data transmission performance in dynamic environments. In particular, the works in [22]–[24] analyzed machine learning based resource management in dynamic wireless network situations. The work in [22] analyzed radio resource scheduling problem with diverse transmission requirements as a Markov decision process (MDP) and demonstrated that reinforcement learning (RL) was an effective solution to the complex problem with dynamics. The authors in [23] proposed RL based dynamic resource allocation method to accommodate high mobility in 5G networks while satisfying heterogeneous user requirements and network architectures. In [24], the authors improved network efficiency via an RL based dynamic power control scheme and verified RL can achieve low protocol overheads for practical applications. Furthermore, the authors in [25]–[28] have studied the use of machine learning for DT optimization in dynamic wireless networks. The work in [25] used RL to minimize the energy consumption of network virtual function (NFV) migrations in a DT network with dynamic NFV communication and computation resource requirements. The authors in [26] used RL to find the optimal target server for DT migration with varying network topologies. The work in [27] proposed a multi-agent RL method to learn the change of vehicular topology and resource requirements of computation tasks, so as to minimize the task offloading costs in DT vehicular network. The authors in [28] used RL to learn the dynamic UAV connection topology and computation task requirements, thereby maximizing the computing resource efficiency by adaptive task assignment in UAV-assisted DT networks. However, the RL methods designed in [25]–[28] cannot adapt to an unseen environment since the hyper-parameters and exploration strategies of the RL methods in [25]–[28] are specifically designed to fit the training tasks in a given environment. Once the RL agent encounters an unseen environment, the specifically trained RL methods may not be able to find an optimal solution. Since DT requires a continuous mapping between the physical and virtual systems, the designed DT optimization methods must adapt to the unseen environment, i.e., dynamic wireless network capacity and unseen physical system status.

B. Contribution

The main contribution of this work is a novel DT framework that enables a base station (BS) to continually optimize

DT synchronization via communication resource scheduling in a dynamic wireless network where the status of physical system changes over time. The contributions of this article include

- We develop a digital network twin framework, where a BS collects physical object state data from wireless devices for the generation of a virtual system. Due to the limited wireless resource blocks (RBs) for DT mapping, only a subset of devices can transmit their data to the BS for virtual system update. Hence, the BS must select a subset of devices and optimize RB allocation for these devices to improve the synchronization between the physical and virtual systems.
- We formulate this device scheduling and RB allocation problem as a constrained Markov process (CMDP) problem whose goal is to minimize the long-term mismatch between the physical system and the virtual system. The packet errors, as well as the dynamics in terms of physical object states and wireless network capacity, are considered in the problem.
- To solve the problem, we first transform the problem into a dual problem that refines the impacts of RB constraints on device scheduling strategies. Then, we propose a continual reinforcement learning (CRL) algorithm to find the optimal device scheduling strategies. In particular, a multi-timescale replay (MTR) buffer is first introduced in the CRL algorithm for extracting common knowledge of strategies from both old and fresh experiences. Next, a modified soft actor critic (SAC) agent is used to enhance the exploration of the scheduling strategies while satisfying RB consumption constraints. With this mechanism, the proposed CRL algorithm can quickly converge to an effective strategy for an unseen physical system status.

Simulations with the Intel Berkeley research lab sensor data and user trajectory locations show that, compared to traditional methods that schedule device at fixed interval time slots, the proposed CRL based device scheduling algorithm can reduce the normalized root mean square error (NRMSE) of the estimated virtual states by up to 55.2%.

The remainder of this paper is organized as follows. The system model and the problem formulation are illustrated in Section II. The proposed CRL algorithm for device scheduling in continual DT synchronization optimization is introduced in Section III. In Section IV, simulation results are presented and discussed. Finally, the conclusions are drawn in Section V.

II. SYSTEM MODEL AND PROBLEM FORMULATION

Consider a DT enabled smart factory in 5G wireless network as shown in Fig. 1, in which a set \mathcal{N} of N devices (i.e. thermo-hygrometers, positioning sensors, monitoring cameras, and LiDARs) monitor factory from different perspectives i.e., room temperatures, robot motions, workstation status, and three-dimensional factory layout. Equipped with edge servers, a BS integrates communication and computational resources to collect sensing data from these devices for DT creation and synchronization [29]. The DT will keep mapping the sensed physical object states into real-time virtual object states,

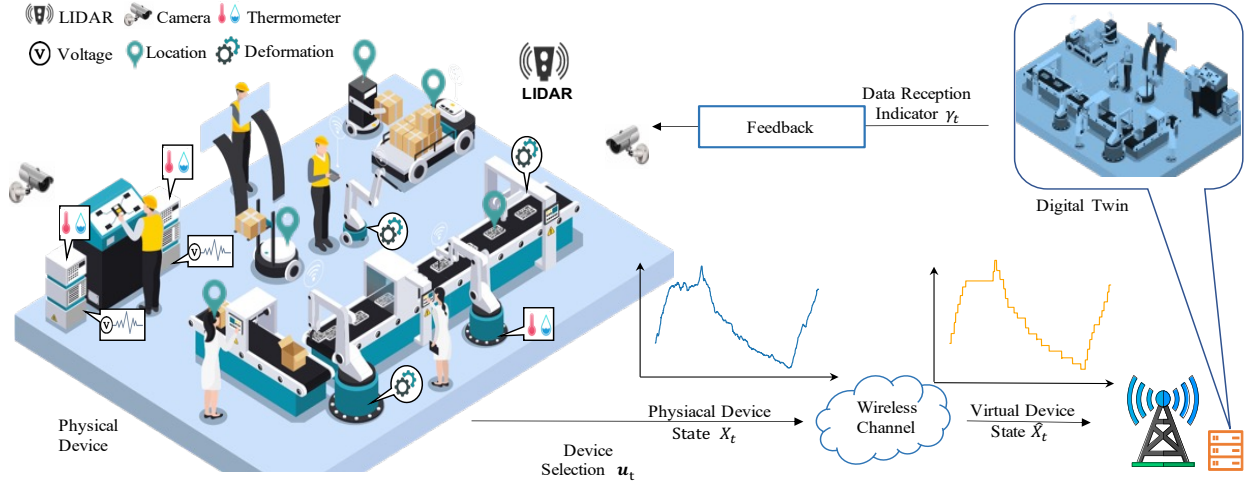


Fig. 1. DT enabled smart factory architecture.

to support continuous simulation and prediction of object behaviors. Notice that, DT mapping mismatch, the difference between the physical states and virtual states, inevitably exists because of the transmission delay and errors. Meanwhile, due to the limited wireless resources, the BS can only selectively schedule a subset of the devices to collect effective sensing data that can revise the DT mapping mismatch.

In the considered system, once the devices are scheduled, they transmit sensing data to the BS via wireless channels. However, due to the inherent uncertainty of wireless channels, packet errors may occur during the sensing data transmission. Hence, in the considered system, the BS can only update the virtual states at DT when the received sensing data does not have errors. After receiving a packet, the BS responds with a feedback message (ACK/NACK). Given the feedback message, the device can obtain the latest virtual state at DT. Only after ACK is fed back, the device is informed that the virtual state has been updated into the most recent transmitted sensing data; otherwise, the virtual state stays. In this way, the device can calculate the DT mapping mismatch by comparing the current observed physical state with the virtual state. When scheduling a device to collect the sensing data, the BS can also collect the DT mismatch information of the device, which can be used to adjust the device schedule policy. Next, we first introduce the mismatch model to measure the synchronization performance of the DT system. Then, we formulate a mismatch minimization problem. Table I provides a summary of the notations in this paper.

A. Mismatch Model

Here we introduce the mismatch model, which is extracted from both physical and virtual states to measure DT synchronization. At discrete transmission time slot t , the BS schedules device n to upload its sampled sensing data $X_{n,t}$ using orthogonal frequency division multiple access (OFDMA). The BS updates the virtual device state $\hat{X}_{n,t}$ at DT with the sensing data $X_{n,t}$. We assume that the BS can allocate a set \mathcal{M} of M uplink orthogonal RBs to the scheduled devices and each RB can be allocated to at most one device. The data rate

TABLE I
LIST OF NOTATIONS

Notation	Description
N	Number of devices
$X_{n,t}$	Physical state of device n at time slot t
$\hat{X}_{n,t}(u_{n,t})$	Virtual state of sensor n at time slot t
$u_{n,t}$	Device selection index for device n at time slot t
$r_{n,t}(u_{n,t})$	Data rate of device n at time slot t
b_n	Number of occupied RBs by device n
ξ_n^{th}	Threshold of mismatch function for device n
W	Bandwidth of each RB
P_n^u	Transmit power of device n
σ_N^2	Variance of AWGN
o_n	Rayleigh fading factor of device n
d_n	Distance between device n to the BS
$h_{n,t}$	Channel gain of device n
L_n	Data size of the sensing data from device n
p_n	Packet error rate of the transmission of device n
m	Waterfall threshold in packet error function
$D_{n,t}(u_{n,t})$	Uplink transmission delay for $X_{n,t}$
$\gamma_{n,t}$	Data reception indicator
$Z_{n,t}(u_{n,t})$	Mismatch of device n at time slot t
$\mathbf{u}_t \in \mathbb{R}^{1 \times N}$	Transmission decision vector of devices
$\mathbf{b}_t \in \mathbb{R}^{1 \times N}$	RB occupation number vector
M	Number of RBs at the BS for DT

of the sensing data uplink transmission from device n to the BS at discrete time slot t is given by (in bits/s)

$$r_{n,t}(u_{n,t}) = u_{n,t} b_n W \log_2 \left(1 + \frac{P_n^u h_{n,t}}{N_0 b_n W} \right), \quad (1)$$

where $u_{n,t} \in \{0, 1\}$ is a device schedule index with $u_{n,t} = 1$ indicating that device n is selected to transmit the sensing data $X_{n,t}$ at time slot t , and $u_{n,t} = 0$, otherwise; b_n is the number of RBs requested by device n from the BS; W is the

bandwidth of each RB; P_n^u is the transmit power of device n ; $h_{n,t} = o_n d_n^{-2}$ is the channel gain with o_n being the Rayleigh fading factor and d_n being the distance between device n and the BS, and N_0 is the noise power spectral density.

Let L_n be the data size of the sensing data of device n , the uplink transmission delay of device n transmitting $X_{n,t}$ to the BS is

$$D_{n,t}(u_{n,t}) = \frac{L_n}{r_{n,t}(u_{n,t})}. \quad (2)$$

The packet error rate is defined as

$$p_n = \mathbb{E}_{h_{n,t}} \left(1 - \exp \left(-\frac{mN_0 b_n W}{P_n^u h_{n,t}} \right) \right), \quad (3)$$

where $\mathbb{E}_{h_{n,t}}(\cdot)$ is the expectation taken over the channel gain $h_{n,t}$ and m is a waterfall threshold [30]. Then, the probability that the BS correctly receives a sensing data packet uploaded by device n is $1 - p_n$. Hence, the data reception indicator $\gamma_{n,t}$ is given by

$$\gamma_{n,t} \sim B(1 - p_n), \quad (4)$$

where $B(\cdot)$ is the Bernoulli distribution function, $\gamma_{n,t} = 1$ indicates the sensing data $X_{n,t}$ of device n is received without errors at time slot t , and $\gamma_{n,t} = 0$, otherwise.

Upon the reception of sensing data, the virtual state at DT $\hat{X}_{n,t}$ is updated with the latest received data, otherwise $\hat{X}_{n,t}$ remains the same as the last time slot, as shown in Fig. 1. Hence, the evolution of the virtual state at DT is given by

$$\hat{X}_{n,t}(u_{n,t}) = \begin{cases} X_{n,t-D_{n,t}(u_{n,t})}, & \gamma_{n,t} = 1, \\ \hat{X}_{n,t-1}(u_{n,t-1}), & \text{otherwise.} \end{cases} \quad (5)$$

In this context, DT synchronization directly requires reducing the mismatch between the physical and virtual states, rather than merely reducing transmission delay. To evaluate DT synchronization, we calculate mismatch between the virtual state $\hat{X}_{n,t}$ and the physical state $X_{n,t}$ of device n at time slot t . Since we consider two types of sensors: 1) thermo-hygrometers and 2) positioning sensors, we use different loss functions to measure their mismatch. The loss function used to measure the temperature mismatch which extracts just noticeable differences (JND) [31] for humans is

$$Z_{n,t}(u_{n,t}) = \max \left\{ \frac{|X_{n,t} - \hat{X}_{n,t}|}{|\hat{X}_{n,t}|} - \xi_n^{\text{th}}, 0 \right\}, n \in \mathcal{N}_J, \quad (6)$$

where ξ_n^{th} is the threshold of device n to filter the insignificant mismatch, \mathcal{N}_J is the device set of thermo-hygrometers, and $u_{n,t}$ is omitted for notational simplicity. The loss function used to measure positioning mismatch [32] is

$$Z_{n,t}(u_{n,t}) = \max \left\{ |X_{n,t} - \hat{X}_{n,t}| - \xi_n^{\text{th}}, 0 \right\}, n \in \mathcal{N}_P, \quad (7)$$

where \mathcal{N}_P is the device set of positioning sensors.

From (4)-(7), we can see that the mismatch $Z_{n,t}$ depends on the physical state $X_{n,t}$, the device selection decision $u_{n,t}$ and packet error rate p_n . As $D_{n,t}$ and p_n increase, the mismatch $Z_{n,t}$ increases. Therefore, to maintain the DT synchronization, the BS must guarantee the timeliness of sensing data transmission through the device scheduling policy

adapting to physical state changes and dynamic transmission environments.

B. Problem Formulation

To consistently maintain DT synchronization, we formulate an optimization problem whose goal is to minimize the weighted mismatch in DT system, considering the diverse transmission priorities of heterogeneous devices (i.e., upheaval temperature data transmission is more urgent than positioning data). This problem is optimized by determining the device scheduling vector \mathbf{u}_t at the BS, given by

$$\mathbb{P}1 : \min_{\mathbf{u}_t} \limsup_{T \rightarrow \infty} \frac{1}{TN} \mathbb{E}_\tau \left(\sum_{t=1}^T \mathbf{w}^\top \mathbf{Z}_t(\mathbf{u}_t) \right) \quad (8)$$

$$\text{s.t. } u_{n,t} \in \{0, 1\}, \quad n \in \mathcal{N}, \quad t \in \mathcal{T}, \quad (8a)$$

$$\lim_{T \rightarrow \infty} \frac{1}{T} \sum_{t=1}^T \mathbb{E}_\tau \left(\mathbf{b}^\top \mathbf{u}_t \mid \mathbf{Z}_0 \right) \leq M, \quad (8b)$$

where $\mathbf{u}_t = [u_{1,t}, \dots, u_{N,t}]^\top$ is the device scheduling vector; $\mathbf{w} = [w_1, \dots, w_N]^\top$ is the transmission priority vector of all devices with w_n being the priority of the sensing data of device n ; $\mathbf{Z}_t(\mathbf{u}_t) = [Z_{1,t}(u_{1,t}), \dots, Z_{N,t}(u_{N,t})]^\top$ is the mismatch vector of all the devices at time slot t ; \mathbf{Z}_0 is the initial mismatch vector at time slot 0. $\tau = [\mathbf{Z}_1(\mathbf{u}_1), \dots, \mathbf{Z}_T(\mathbf{u}_T)]$ is the evolution trajectory of the mismatch vector determined by \mathbf{u}_t ; \mathcal{T} is the set of all considered time slots; $\mathcal{N} = \mathcal{N}_J \cup \mathcal{N}_P$ is the set of all devices; $\mathbf{b} = [b_1, \dots, b_N]^\top$ is the vector of the occupied RB numbers by each device in \mathcal{N} ; and M is the total number of the RBs of the BS which is inadequate to schedule all devices at the same time. Constraints (8a) and (8b) indicate that the BS can allocate at most 1 RB to each device each time, and at most M RBs to the scheduled devices overall. From (8), we can see that the device scheduling decision \mathbf{u}_t and physical states X_t determine the DT mismatch and the device scheduling decision \mathbf{u}_t must satisfy the limited RB number constraint for the given X_t and \mathbf{b} .

However, one can notice that the problem (8) is challenging to solve via conventional optimization methods for the following reasons. First, from (5)-(7) we see that, since the evolution of mismatch $Z_{n,t}$ is determined by the sequence of device scheduling vector \mathbf{u}_t , the problem (8) belongs to CMDP [33] and is hard to be solved by conventional optimization methods. Second, the BS must know the mismatch vector \mathbf{Z}_t of all devices to optimize device scheduling vector \mathbf{u}_t . However, \mathbf{Z}_t is calculated at each device, hence the BS can only observe partial \mathbf{Z}_t from the scheduled devices, and cannot obtain $Z_{n,t}$ of the unscheduled devices. The partial observation makes the BS infeasible to solve the problem via optimization methods. Third, the total available RB number M may change with wireless environment dynamics during the prolonged DT mapping [34]. However, conventional optimization methods do not consider variable M , and need to be re-implemented once M changes. The dynamic programming (DP) and standard reinforcement learning (RL) methods can help learn device scheduling strategies in dynamic environments, but need to be enhanced in regards to their

few shot performances with the ever-changing environments. Thus, we propose a CRL algorithm to learn and adjust device scheduling strategies with in-depth analysis on impacts of the constraints M over the device scheduling vector \mathbf{u}_t , and quick adaptivity ability refined from historical experiences at multiple timescales.

III. PROPOSED CRL ALGORITHM FOR CMDP

In this section, we introduce the proposed CRL algorithm, which integrates MTR [35] into an SAC framework [36]. We will first transform the original long-term-constrained device scheduling problem (8) into a Lagrangian dual problem, such that the goal of the considered system is to seek a prime-dual solution with refined constraints on optimization variables [33]. Then, the multiple timescale replay for soft actor critic (MTR-SAC) enabled CRL algorithm will solve the non-convex dual problem considering the dynamic and unpredictable physical system status. An MTR buffer is integrated into the CRL algorithm to store experiences at different timescales, thus the CRL can learn a stable policy across the historical stages for adapting to unknown dynamics. Meanwhile, the SAC framework enhances the action sampling efficiency with maximizing the logarithmic formatted action entropy. In what follows, we first explain how to transform the problem (8) into a Lagrangian dual problem. Then, we introduce components of the proposed CRL algorithm. Finally, we explain the training procedure of the proposed CRL algorithm.

A. Lagrangian Transform

Since constraint (8b) in problem (8) is the expectation of the long-term consumed RBs, it may lead to temporary overbudget RB consumption, i.e. $\mathbf{b}_t^\top \mathbf{u}_t > M$. However, even a temporary resource overbudget can strain the available RBs and lead to congestion. Such congestion in practice increases the data packet error rate thus breaking down the DT mapping. With such consideration, we transform the expectation-wise constraint (8b) into a state-wise constraint [36], to maintain under-budget device scheduling.

1) *State-wise Constrained Problem*: The state-wise constraint is given by [36]

$$V_c(\mathbf{Z}_t(\mathbf{u}_t)) = \lim_{T \rightarrow \infty} \frac{1}{T} \mathbb{E}_\tau \left(\sum_{t=1}^T \mathbf{b}^\top \mathbf{u}_t \mid \mathbf{Z}_0 = \mathbf{Z}_t(\mathbf{u}_t) \right) \leq M, \forall \mathbf{Z}_t \in \mathcal{I}_F, \quad (9)$$

where $\mathcal{I}_F = \mathcal{I} \cap \mathcal{S}_F$ is the feasible region, with \mathcal{I} being the set of all possible initial mismatch vector \mathbf{Z}_0 and \mathcal{S}_F being the feasible set of \mathbf{Z}_t . Compared to constraint (8b), the state-wise constraint (9) regards each mismatch vector \mathbf{Z}_t as an initial point in (8b), because the constraint (8b) considers $T \rightarrow \infty$. Hence, the problem with state-wise constraint is

$$\mathbb{P}2: \quad \min_{\mathbf{u}_t} \limsup_{T \rightarrow \infty} \frac{1}{TN} \mathbb{E}_\tau \left(\sum_{t=1}^T \mathbf{w}^\top \mathbf{Z}_t(\mathbf{u}_t) \right) \quad (10)$$

$$\text{s.t. } V_c(\mathbf{Z}_t(\mathbf{u}_t)) \leq M, \forall \mathbf{Z}_t \in \mathcal{I}_F. \quad (10a)$$

Since the state-wise constraint (10a) takes each mismatch vector $\mathbf{Z}_t(\mathbf{u}_t)$ as an initial point, the consumed RB number $\mathbf{b}_t^\top \mathbf{u}_t$ temporarily exceeding M violates the constraint (10a). In this way, $\mathbb{P}2$ has a stricter constraint than $\mathbb{P}1$ to guarantee under budget resource consumption, and the optimal solution of $\mathbb{P}2$ will be sub-optimal to $\mathbb{P}1$. However, considering the fact that the optimal solution of $\mathbb{P}1$ can lead to a temporary overconsumption of resources, the optimal solution of $\mathbb{P}2$ will be the one that identifies the practically feasible optimal solution.

2) Lagrangian Dual of State-wise Constrained Problem:

Since the state-wise constraint (10a) forces a constraint for each \mathbf{Z}_t in \mathcal{I}_F , we employ one corresponding Lagrangian multiplier on each \mathbf{Z}_t and denote $\lambda(\mathbf{Z}_t)$ as the multiplier of each \mathbf{Z}_t [36]. Therefore, taking into account $\mathbf{Z}_t \in \mathcal{I}_F$, the original state-wise Lagrangian function $\mathcal{L}_{\text{o-stw}}(\mathbf{u}, \lambda)$ of problem $\mathbb{P}2$ is

$$\mathcal{L}_{\text{o-stw}}(\mathbf{u}, \lambda) = \limsup_{T \rightarrow \infty} \frac{1}{T} \mathbb{E}_\tau \left(\sum \frac{1}{N} \mathbf{w}^\top \mathbf{Z}_t(\mathbf{u}_t) \right) + \sum_{\mathbf{Z}_t \in \mathcal{I}_F} \lambda(\mathbf{Z}_t(\mathbf{u}_t)) \left[V_c(\mathbf{Z}_t(\mathbf{u}_t)) - M \right], \quad (11)$$

where $\lambda(\mathbf{Z}_t(\mathbf{u}_t))$ is the state-wise multiplier for each \mathbf{Z}_t . Different from the traditional Lagrangian method that assigns one λ to all \mathbf{Z}_t [37], $\mathcal{L}_{\text{o-stw}}(\mathbf{u}, \lambda)$ applies different Lagrangian multipliers to each \mathbf{Z}_t , with which the infeasible \mathbf{Z}_t values can be indicated.

Notice that it is hard to demarcate the feasible region \mathcal{I}_F , while impractical to find the summation of infinite set \mathcal{I}_F . In such context, we use experience sampling based learning method to transform $\mathcal{L}_{\text{o-stw}}(\mathbf{u}, \lambda)$ into an equivalent form $\mathcal{L}_{\text{stw}}(\mathbf{u}, \lambda)$, which is given by

$$\mathcal{L}_{\text{stw}}(\mathbf{u}, \lambda) = \mathbb{E}_{\mathbf{Z} \sim d_0(\mathbf{Z})} \left[\frac{1}{N} \mathbf{w}^\top \mathbf{Z}_t(\mathbf{u}_t) + \lambda(\mathbf{Z}_t(\mathbf{u}_t)) (V_c(\mathbf{Z}_t(\mathbf{u}_t)) - M) \right], \quad (12)$$

where $d_0(\mathbf{Z})$ is the statistical distribution of \mathbf{Z}_t obtained by sampling method. The proof of the equivalence of optimizing $\mathcal{L}_{\text{stw}}(\mathbf{u}, \lambda)$ and $\mathcal{L}_{\text{o-stw}}(\mathbf{u}, \lambda)$ is illustrated by *Theorem 1*.

Theorem 1 If the Lagrangian dual problem of $\mathcal{L}_{\text{stw}}(\mathbf{u}, \lambda)$, which is $\max_\lambda \inf_{\mathbf{u}} \mathcal{L}_{\text{stw}}(\mathbf{u}, \lambda)$, has the optimal scheduling vector sequence \mathbf{u}^* and Lagrange multiplier λ^* , then \mathbf{u}^* is also the optimal scheduling vector sequence for the state-wise constrained problem $\mathbb{P}2$.

Proof: See Appendix A. ■

With *Theorem 1*, the equivalent dual problem of $\mathbb{P}2$ is given by [38]

$$\mathbb{P}3: \max_{\lambda} \inf_{\mathbf{u}} \mathcal{L}_{\text{stw}}(\mathbf{u}, \lambda) \quad \text{s.t. } \lambda \geq 0. \quad (13)$$

Since we consider the real-word physical states X_t change with unpredictable dynamics, $\mathbf{Z}_t(\mathbf{u}_t)$ is usually non-convex to \mathbf{u}_t , making it hard to solve the problem $\mathbb{P}3$ by convex optimization or DP approach. Moreover, the changing of M leads to varying environments that severely affects the performance

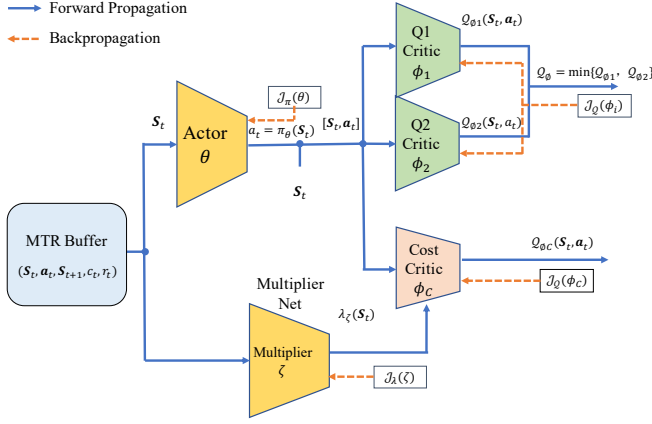


Fig. 2. Architecture of the proposed MTR-SAC method.

of standard RL methods. Hence, to solve problem $\mathbb{P}3$, we employ a CRL algorithm to learn a device scheduling policy \mathbf{u} and the multiplier function $\lambda(\mathbf{Z}_t)$ which adapts to dynamic X_t and M via learning from the sampled experiences.

B. Components of the CRL Algorithm

The proposed CRL algorithm uses multi-timescale replay for soft actor-critic (MTR-SAC) agent. A standard SAC model consists of two important modules, actor-critic network module, and replay buffer module. With these two modules, SAC can be trained with temporal-difference (TD) error and experience replay, respectively, thus achieving high learning efficiency with limited training data [39]. Moreover, through maximizing action entropy, SAC learns a more stochastic policy compared to other standard RL such as deep Q-network (DQN) [39]. MTR is introduced as a data rehearsal scheme that balances the amounts of long-term and short-term memory in the replay buffer, thus realizing continual learning across dynamic environments [35]. Next, we will introduce components of the proposed MTR-SAC method.

The MTR-SAC method consists of the following components: 1) Agent, 2) State, 3) Action, 4) Policy, 5) Reward, 6) Cost, 7) MTR buffer, and 8) Multiplier function, which are elaborated as follows:

- **Agent:** The agent performs the proposed method is the BS that consecutively schedule devices for uplink sensing data transmission.
- **State:** The state at the BS is defined as $\mathbf{S}_t = [s_{1,t}, \dots, s_{N,t}]$, where $s_{n,t} = [\Phi_{n,t}(u_{n,t}), Y_{n,t}, \gamma_t]$ is the status of each device n at time slot t , with $\Phi_{n,t}(u_{n,t}) = t - g_{n,t}^m$ being the time span since the last time when data from device n is correctly received by the BS, $g_{n,t}^m = \sup\{t \mid \gamma_{n,t} = 1\}$ being the latest time slot when the data from device n is correctly accepted, and $Y_{n,t} = Z_{n,g_{n,t}^m}$ being the latest received mismatch value. Notice that, $\Phi_{n,t}(u_{n,t})$ and $\gamma_{n,t}$ can be calculated at the BS, while $Y_{n,t}$ will be transmitted to the BS along with the sensing data.
- **Action:** The action of BS is the scheduling index $u_{n,t}$ for each device n , at each time slot t . In particular, $u_{n,t} = 1$ indicates the device n is scheduled to transmit data

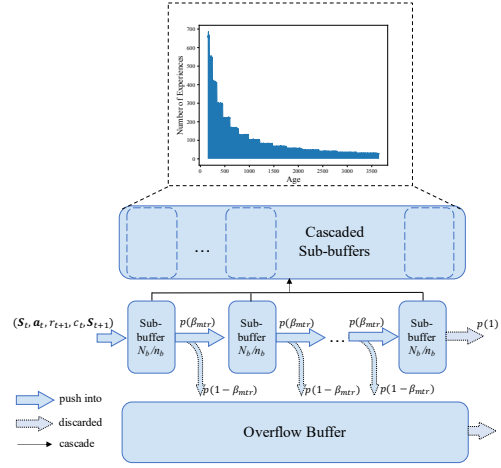


Fig. 3. Architecture of MTR buffer.

with b_n allocated RBs at time slot t , while $u_{n,t} = 0$ indicates that the device n remains idle at time slot t . The vector of BS's actions at time slot t is captured in $\mathbf{a}_t = [u_{1,t}, \dots, u_{N,t}]^\top$.

- **Policy:** The policy $\pi_\theta(\mathbf{a}_t \mid \mathbf{S}_t)$ is the probability that the BS chooses an action \mathbf{a}_t at state \mathbf{S}_t , where the policy is implemented at the actor network with a neural network (NN) parameterized by θ , as shown in Fig. 2.
- **Reward:** The reward is used to capture the mismatch of all devices in the DT system when a device scheduling action \mathbf{a}_t is operated at state \mathbf{S}_t . Since the BS schedules devices and allocate RBs centrally, we define a reward function of the whole DT system as

$$\begin{aligned} r(\mathbf{S}_t, \mathbf{a}_t) &= -\frac{1}{N} \mathbf{w}^\top \mathbf{Z}_t(\mathbf{u}_t) \\ &= -\frac{1}{N} \sum_{n=1}^N w_n Z_{n,t}(u_{n,t}), \end{aligned} \quad (14)$$

where w_n is the transmission priority weight of device n . From (14) we see that the reward $r(\mathbf{S}_t, \mathbf{a}_t)$ increases as the mismatch decrease, hence maximizing the reward leads to minimized weighted mismatch in the DT. Since the BS can only observe partial \mathbf{Z}_t from the scheduled devices, the complete \mathbf{Z}_t is supplemented with a certain delay after subsequent data collection by BS and is stored in the replay buffer specifically for the model training. As shown in Fig. 2, the reward in the proposed method is regressed by NN based reward value functions $Q_{\phi_i}(\mathbf{S}_t, \mathbf{a}_t)$, $i \in \{1, 2\}$ at the critic networks, where ϕ_i is the NN parameters.

- **Cost:** The cost captures the consumed RB number when a scheduling action \mathbf{a}_t is operated at state \mathbf{S}_t . Consider the RB number constraint M , the cost is defined as

$$c(\mathbf{S}_t, \mathbf{a}_t) = \begin{cases} M, & \mathbf{b}^\top \mathbf{a}_t \leq M, \\ \mathbf{b}^\top \mathbf{a}_t, & \mathbf{b}^\top \mathbf{a}_t > M. \end{cases} \quad (15)$$

Based on this definition, the extent of an action violating the RB constraints is represented by $c(\mathbf{S}_t, \mathbf{a}_t) - M$. The purpose of the cost definition is to evaluate the penalty of violating constraints separately from reward, so that the

changing constraints do not influence the reward formula. The cost in the proposed method is regressed by NN based cost value functions $Q_{\phi_C}(\mathbf{S}_t, \mathbf{a}_t)$ at cost critic network, where ϕ_C is the NN parameters, as shown in Fig. 2.

- **MTR buffer:** The MTR buffer stores the experiences at different timescales and consists of n_b cascaded first in first out (FIFO) sub-buffers and a separate overflow buffer, as shown in Fig. 3. Any new experiences $(\mathbf{S}_t, \mathbf{a}_t, r_t, c_t, \mathbf{S}_{t+1})$ are first pushed into the first sub-buffer. As long as a sub-buffer is full, the oldest experience in the sub-buffer is popped out, then be pushed into the next sub-buffer with probability β_{mtr} or be discarded to the overflow buffer with probability $1 - \beta_{mtr}$. The overflow buffer is used to stabilize the total number of experiences in MTR buffer when the cascaded sub-buffers are not full in the early training stage. When the overflow buffer has N_b discarded experiences, the overflow buffer is full and shrunk with the oldest experiences being thoroughly removed, until the whole MTR buffer has at most N_b experiences. After all cascaded sub-buffers are full, the overflow buffer will be empty, and the distribution of the experience age in the cascaded sub-buffers results in a power law distribution of memories [35]. Hence, the samples of the experiences in MTR buffer can balance multi-timescale environment characteristic with containing abundant fresh experiences and a few old experiences.
- **Multiplier function:** The multiplier function is the mapping relationship from each state \mathbf{S}_t to the corresponding Lagrange multiplier value [36]. The multiplier function is implemented at the multiplier network with a NN and can be defined as $\lambda_\zeta(\mathbf{S}_t)$, where ζ is the NN parameters. Given the definition, the BS can use experience samplings to obtain a estimation of $\mathcal{L}_{\text{stw}}(\mathbf{u}, \lambda)$ in (12), given by

$$\widehat{\mathcal{L}}_{\text{stw}} = \mathbb{E}_{\mathbf{S}} [r(\mathbf{S}_t, \mathbf{a}_t) - \lambda_\zeta(\mathbf{S}_t) (c(\mathbf{S}_t, \mathbf{a}_t)) - M], \quad (16)$$

where $\mathbb{E}_{\mathbf{S}}(\cdot)$ is the expectation taken over the sampled \mathbf{S}_t in MTR buffer. Then the MTR-SAC method is trained to maximize $\widehat{\mathcal{L}}_{\text{stw}}$.

C. Training of the MTR-SAC Method

Given the above MTR-SAC components, we next introduce the entire procedure of training the proposed MTR-SAC method. We first define the loss functions of the critic, actor, and multiplier networks within the proposed MTR-SAC framework. Then we explain how this CRL solution is trained.

1) *Loss function of value (critic) networks:* The loss function to train the two reward value functions $Q_{\phi_i}(\mathbf{S}_t, \mathbf{a}_t)$ is given by [39]

$$J_Q(\phi_i) = \mathbb{E}_{(\mathbf{S}_t, \mathbf{a}_t) \sim \mathcal{B}} \left[\frac{1}{2} \left(Q_{\phi_i}(\mathbf{S}_t, \mathbf{a}_t) - \mathbb{E}_{\mathbf{a}_{t+1} \sim \pi} \left(r(\mathbf{S}_t, \mathbf{a}_t) + \gamma Q_{\bar{\phi}_i}(\mathbf{S}_{t+1}, \mathbf{a}_{t+1}) \right) \right)^2 \right], \quad (17)$$

where $i \in \{1, 2\}$ is the index of the critic networks as show in Fig. 2; \mathcal{B} is the MTR replay buffer; $\bar{(\cdot)}$ is the target network with a lower update frequency than the original network [40]; and γ is the reward discounted factor. The stochastic gradient of $J_Q(\phi_i)$ can be given by

$$\widehat{\nabla}_{\phi_i} J_Q(\phi_i) = \nabla_{\phi_i} Q_{\phi_i}(\mathbf{S}_t, \mathbf{a}_t) \left[Q_{\phi_i}(\mathbf{S}_t, \mathbf{a}_t) - \left(r(\mathbf{S}_t, \mathbf{a}_t) + \gamma Q_{\bar{\phi}_i}(\mathbf{S}_{t+1}, \mathbf{a}_{t+1}) \right) \right]. \quad (18)$$

The loss function of $Q_{\phi_C}(\mathbf{S}_t, \mathbf{a}_t)$ is

$$J_Q(\phi_C) = \mathbb{E}_{(\mathbf{S}_t, \mathbf{a}_t) \sim \mathcal{B}} \left[\frac{1}{2} \left(Q_{\phi_C}(\mathbf{S}_t, \mathbf{a}_t) - \left(c(\mathbf{S}_t, \mathbf{a}_t) + \gamma_C \mathbb{E}_{\mathbf{a}_{t+1} \sim \pi} Q_{\bar{\phi}_C}(\mathbf{S}_{t+1}, \mathbf{a}_{t+1}) \right) \right)^2 \right], \quad (19)$$

where γ_C is cost discount factor. The stochastic gradient to optimize $J_Q(\phi_C)$ is given by

$$\widehat{\nabla}_{\theta} J_Q(\phi_C) = \nabla_{\phi_C} Q_{\phi_C}(\mathbf{S}_t, \mathbf{a}_t) \times \left[Q_{\phi_C}(\mathbf{S}_t, \mathbf{a}_t) - \left(c(\mathbf{S}_t, \mathbf{a}_t) + \gamma_C Q_{\bar{\phi}_C}(\mathbf{S}_t, \mathbf{a}_t) \right) \right]. \quad (20)$$

2) *Loss function of the policy (actor) network:* As the wireless network capacity fluctuates over time, to maintain DT synchronized, the device scheduling policy needs to be continuously adjusted with the changes on the number available RBs (i.e. M). The MTR buffer provides the access to former (fresh and old) device scheduling experiences with different RB constraints, such that the policy function will be trained with invariant risk minimization (IRM) scheme over common distributions learned from these historical experiences. The IRM scheme encourages the policy to learn a state-to-action mapping that is invariant across all possible networking environments, and if the mapping is stable across a large number of different environments, the mapping will be more likely to perform well in the unseen environments [35]. In such context, the loss of IRM actor is given by

$$J_\pi^{\text{IRM}}(\theta) = \left\| \nabla_{w|w=1} J_\pi^e(\theta, w \cdot \pi) \right\|^2, \quad (21)$$

within which $J_\pi^e(\theta, w \cdot \pi)$ is the loss function of the original SAC policy function parameterized by θ under environment e , with $w \cdot \pi$ being a stable policy across multiple environments, and w is a dummy variable [41]. The term $\nabla_{w|w=1} J_\pi^e(\theta, w \cdot \pi)$ is the derivative of $J_\pi^e(\theta, w \cdot \pi)$ at $w = 1$, which indicates how much the actor network loss changes as the policy changes, thus the term $\nabla_{w|w=1} J_\pi^e(\theta, w \cdot \pi)$ can be used to measure the performance of the dummy policy $w \cdot \pi$ at each environment e . Hence, minimizing $J_\pi^{\text{IRM}}(\theta)$ can reduce the policy π intrinsically change along with new environments, thus mitigating catastrophic forgetting.

The original SAC actor network loss function $J_\pi^{\text{SAC}}(\theta)$ is

$$J_\pi^{\text{SAC}}(\theta) = \mathbb{E}_{\mathbf{S}_t \sim \mathcal{B}} \left\{ \mathbb{E}_{\mathbf{a}_t \sim \pi} \left[\alpha \log(\pi(\mathbf{a}_t | \mathbf{S}_t)) - Q_\phi(\mathbf{S}_t, \mathbf{a}_t) + \lambda_\zeta(\mathbf{S}_t) (Q_{\phi_C}(\mathbf{S}_t, \mathbf{a}_t) - M) \right] \right\}, \quad (22)$$

where α is the weight of action entropy, $Q_\phi(\mathbf{S}_t, \mathbf{a}_t) = \min\{Q_{\phi_1}(\mathbf{S}_t, \mathbf{a}_t), Q_{\phi_2}(\mathbf{S}_t, \mathbf{a}_t)\}$ is the Q value derived from the two reward value functions, $\lambda_\zeta(\mathbf{S}_t)$ is the estimated multiplier value, and $Q_{\phi_C}(\mathbf{S}_t, \mathbf{a}_t)$ is the estimated cost value.

The loss function $J_\pi(\theta)$ of MTR-SAC actor network is given by

$$J_\pi(\theta) = J_\pi^{SAC}(\theta) + \lambda_{IRM} \sum_{i=1}^{n_b} \frac{|\mathcal{D}_i|}{|\mathcal{D}_{MTR}|} \times \mathbb{E}_{\mathbf{S}_t^i \sim \mathcal{D}_i} \left[\left\| \nabla_{w|w=1} J_\pi^{SAC}(\theta, w \cdot \pi, \mathbf{S}_t^i) \right\|^2 \right], \quad (23)$$

in which λ_{IRM} is the weight coefficient that balances the original actor loss $J_\pi^{SAC}(\theta)$ and the loss of IRM actor $J_\pi^{IRM}(\theta)$, \mathcal{D}_i is the set of experiences in the sub-buffer i with $|\mathcal{D}_i|$ being the number of experiences, $|\mathcal{D}_{MTR}|$ is the total number of experiences in all the MTR buffer. Hence, the second term in (23) indicates the performance of the policy in the environments at different timescales.

To obtain the gradient of the actor network, the policy is represented by a NN transformation form $\mathbf{a}_t = f_\theta(\epsilon_t; \mathbf{S}_t)$, with ϵ_t being an input noise vector sampled from a fixed Gaussian distribution [39], since the target of $J_\pi^{SAC}(\theta)$ is the Q-function learned by differentiable NNs. Take the NN transformation into the policy loss and then, the estimated policy gradient of the original SAC $J_\pi^{SAC}(\theta)$ is

$$\begin{aligned} \hat{\nabla}_\theta J_\pi^{SAC}(\theta) &= \nabla_{\theta} \alpha \log(\pi(\mathbf{a}_t | \mathbf{S}_t)) \\ &+ \left[\nabla_{\mathbf{a}_t} \alpha \log(\pi(\mathbf{a}_t | \mathbf{S}_t)) \right. \\ &- \nabla_{\mathbf{a}_t} \left(Q_\phi(\mathbf{S}_t, \mathbf{a}_t) + \lambda_\zeta(\mathbf{S}_t) Q_{\phi_C}(\mathbf{S}_t, \mathbf{a}_t) \right) \\ &\left. \times \nabla_{\theta} f_\theta(\epsilon_t; \mathbf{S}_t) \right], \end{aligned} \quad (24)$$

where M is neglected since it is irrelevant to θ . Given $\hat{\nabla}_\theta J_\pi^{SAC}(\theta)$, the gradient of the MTR-SAC method is

$$\begin{aligned} \hat{\nabla}_\theta J_\pi(\theta) &= \hat{\nabla}_\theta J_\pi^{SAC}(\theta) + \lambda_{IRM} \sum_{i=1}^{n_b} \frac{|\mathcal{D}_i|}{|\mathcal{D}_{MTR}|} \\ &\times \hat{\nabla}_\theta \left[\left\| \nabla_{w|w=1} J_\pi^{SAC}(\theta, w \cdot \pi, \mathbf{S}_t^i) \right\|^2 \right]. \end{aligned} \quad (25)$$

3) *Loss function of the multiplier network:* The loss function of multiplier network is given by

$$J_\lambda(\zeta) = \mathbb{E}_{\mathbf{S}_t \sim \mathcal{B}} \left\{ \mathbb{E}_{\mathbf{a}_t \sim \pi} [\lambda_\zeta(\mathbf{S}_t) (Q_{\phi_C}(\mathbf{S}_t, \mathbf{a}_t) - M)] \right\}, \quad (26)$$

where the entropy and reward value function term are neglected since the irrelevance with multiplier λ [42]. The stochastic gradient of λ can be given by

$$\hat{\nabla} J_\lambda(\zeta) = (Q_{\phi_C}(\mathbf{S}_t, \mathbf{a}_t) - M) \nabla_\zeta \lambda_\zeta(\mathbf{S}_t). \quad (27)$$

4) *Training process of the MTR-SAC algorithm:* As summarized in Algorithm 1, starting with initial actor θ , critic ϕ , and multiplier networks ζ , the algorithm interacts with the physical networks and uses the achieved state transitions $(\mathbf{S}_t, \mathbf{a}_t, \mathbf{S}_{t+1})$ and regressed values $r(\mathbf{S}_t, \mathbf{a}_t)$ and $c(\mathbf{S}_t, \mathbf{a}_t)$ to calculate the loss functions (17), (19), and (22). It then uses a mini-batch training mechanism to update value networks. Then, based on the sampled interaction experiences in the MTR buffer, it updates the policy network every m_π gradient

Algorithm 1 Training process of the MTR-SAC algorithm

```

1: Input:  $\phi_1, \phi_2, \phi_C, \theta, \zeta$ 
2: Initialize:  $\mathcal{B} \leftarrow \emptyset, \hat{\diamond} \leftarrow \diamond$  for  $\diamond \in \{\phi_1, \phi_2, \phi_C, \theta\}$ 
3: for each episode do
4:   for each environment interaction time slot do
5:     BS obtain  $\mathbf{S}_t, \mathbf{a}_t, \mathbf{S}_{t+1}, r(\mathbf{S}_t, \mathbf{a}_t), c(\mathbf{S}_t, \mathbf{a}_t)$  and fill the MTR buffer by
6:      $\mathbf{a}_t \sim \pi_\theta(\mathbf{a}_t | \mathbf{S}_t), \mathbf{S}_{t+1} \sim p(\mathbf{S}_{t+1} | \mathbf{S}_t, \mathbf{a}_t), \mathcal{B} \leftarrow \mathcal{B} \cup \{(\mathbf{S}_t, \mathbf{a}_t, r(\mathbf{S}_t, \mathbf{a}_t), c(\mathbf{S}_t, \mathbf{a}_t), \mathbf{S}_{t+1})\}$ 
7:   end for
8:   for each gradient step do
9:     update value networks by
10:     $\phi_i \leftarrow \phi - \beta_Q \hat{\nabla}_{\phi_i} J_Q(\phi_i)$  for  $i \in \{1, 2, C\}$ 
11:   if gradient steps mod  $m_\pi = 0$  then
12:     update the policy network by
13:      $\theta \leftarrow \theta - \beta_\pi \hat{\nabla}_\theta J_\pi(\theta)$ 
14:     adjust the temperature by
15:      $\alpha \leftarrow \alpha - \beta_\alpha \hat{\nabla}_\alpha J_\alpha(\alpha)$ 
16:   end if
17:   if gradient steps mod  $m_\lambda = 0$  then
18:     update the multiplier network by
19:      $\zeta \leftarrow \zeta + \beta_\lambda \nabla_\zeta J_\lambda(\zeta)$ 
20:   end if
21:   update the target networks by
22:    $\hat{\diamond} \leftarrow \rho \diamond + (1 - \rho) \diamond$  for  $\diamond \in \{\phi_1, \phi_2, \phi_C, \theta\}$ 
23: end for
24: Output:  $\phi_1, \phi_2, \phi_C, \theta, \zeta$ 

```

steps, and updates the multiplier network every m_λ gradient steps. Such trial, error, then update procedure will be repeated, until the convergence is reached. In Algorithm 1, $\beta_Q, \beta_\pi, \beta_\alpha, \beta_\lambda$, and ρ are learning rates of corresponding NNs.

D. Convergence, Implementation, and Complexity Analysis

In this section, we analyze the convergence, implementation and complexity of the proposed MTR-SAC based CRL device scheduling method.

1) *Convergence Analysis:* For the CMDP in (8) in dynamic environments, we cannot give the optimal solution that the proposed algorithm reaches. Next, using the result of [39, Theorem 1], we can prove that the proposed algorithm will not diverge and can converge to a fixed solution of problem (10) in a static environment, as shown in the following

Lemma 1: *The proposed MTR-SAC method is guaranteed to converge if the following conditions are satisfied 1) reward value function $Q(\mathbf{S}_t, \mathbf{a}_t)$ is bounded, and 2) $Q^{\pi_{new}}(\mathbf{S}_t, \mathbf{a}_t) \geq Q^{\pi_{old}}(\mathbf{S}_t, \mathbf{a}_t)$ holds for feasible \mathbf{S}_t and \mathbf{a}_t with π_{new} being the updated new policy from the old policy π_{old} in each iteration.*

Proof. The proposed MTR-SAC satisfies the two conditions for the following reasons. First, since the actor network is differentiable NN [39], the value of $J_\pi^{IRM}(\theta)$ is bounded, and the finite dimension of \mathbf{a}_t guarantees the action entropy is bounded. Hence the $Q(\mathbf{S}_t, \mathbf{a}_t)$ is bounded and satisfies the condition 1).

Second, the case $J_{\pi_{old}}(\pi_{new}(\cdot | \mathbf{S}_t)) \leq J_{\pi_{old}}(\pi_{old}(\cdot | \mathbf{S}_t))$ always holds in the static environment because we can always

TABLE II
SIMULATION PARAMETERS

Parameter	Value	Parameter	Value
N	20	M	18
W	180kHz	L_n	250B
P_n^u	0.5W	m	0.023dB
N_0	-175 dBm/Hz	ξ^{th}	1×10^{-2}
β_Q, β_π	3×10^{-4}	$\beta_\alpha, \beta_\lambda$	1×10^{-5}
ρ	5×10^{-3}	N_l	3
h_{in}, h_{out}	$4N, N$	h_1, h_2, h_3	256
β_{mtr}	0.8	λ_{IRM}	1×10^{-2}
n_b	4	N_b	5×10^3
m_π	2	m_λ	12

choose $\pi_{\text{new}} = \pi_{\text{old}} \in \Pi$ for the invariant distribution of \mathcal{D}_i . And because the second term in (22) is only relative to the parameter θ , according to the Lemma 2 in [39], the above inequality can be reduced to

$$\begin{aligned} & \mathbb{E}_{\mathbf{a}_t \sim \pi_{\text{new}}} [\log \pi_{\text{new}}(\mathbf{a}_t | \mathcal{S}_t) - Q^{\pi_{\text{old}}}(\mathcal{S}_t, \mathbf{a}_t)] \\ & \leq \mathbb{E}_{\mathbf{a}_t \sim \pi_{\text{old}}} [\log \pi_{\text{old}}(\mathbf{a}_t | \mathcal{S}_t) - Q^{\pi_{\text{old}}}(\mathcal{S}_t, \mathbf{a}_t)]. \end{aligned} \quad (28)$$

Given (28), consider the soft Bellman equation, it can be obtained that $Q^{\pi_{\text{old}}}(\mathcal{S}_t, \mathbf{a}_t) \leq Q^{\pi_{\text{new}}}(\mathcal{S}_t, \mathbf{a}_t)$, which satisfies the condition 2). ■

2) *Implementation Analysis*: Next, we explain the implementation of the proposed MTR-SAC method. The devices use the feedback message from the BS to obtain the virtual state \hat{X}_t , and then calculate the mismatch value $Z_{n,t}$. The BS can only obtain the mismatch value $Z_{n,t}$ by scheduling device n , as $Z_{n,t}$ is transmitted to the BS along with the sensing data packets. Since the BS can not collect real-time $Z_{n,t}$ of all devices due to limited RBs, the BS must record the last received mismatch value $Z_{n,g_{n,t}^m}$ as an estimation of $Z_{n,t}$. Meanwhile, the BS records the last received packet from the devices, such that it can calculate $\Phi_{n,t}(u_{n,t})$ as well as the packet reception indicator $\gamma_{n,t}$. When the resource budget changes, the BS can obtain the total number of available RBs M for device scheduling. In other words, the BS is capable of accessing the necessary information and computation capability to train and deploy the proposed algorithm.

3) *Complexity Analysis*: The time complexity of training and inferring the algorithm is mainly determined by the size of the NN weights [43]. Let N_l be the total number of layers in each NN in SAC module, h_i be the number of neurons in layer l_i , h_{in} be the dimension of the input, and h_{out} be the dimension of the output. Thus, the time complexity of inferring the proposed algorithm can be calculated by $\mathcal{O}(h_{in}h_1 + \sum_{i=1}^{N_l-1} h_i h_{i+1} + h_{out}h_{N_l})$. In the training stage, the MTR-SAC method additionally runs the MTR buffer $J_\pi^{IRM}(\theta)$. The operation of MTR buffer includes pushing in and popping out one experience, thus having the time-complexity of $\mathcal{O}(n_b)$. The time complexity of the training policy network is $\mathcal{O}(h_{in}h_1 + \sum_{i=1}^{N_l-1} h_i h_{i+1} + h_{out}h_{N_l} + n_b)$.

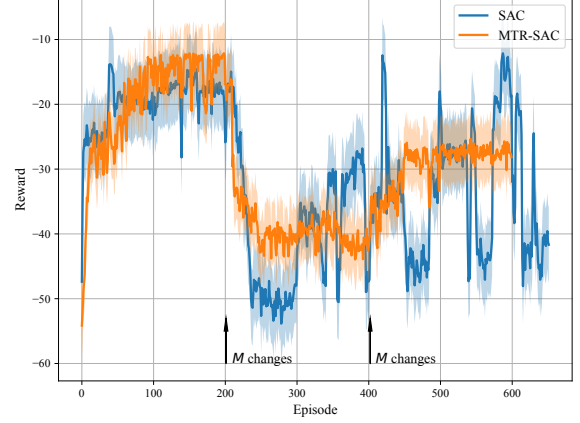


Fig. 4. Convergence of the MTR-SAC method with variable numbers of RBs. The number of available RBs changes from 30, to 10, and then 26.

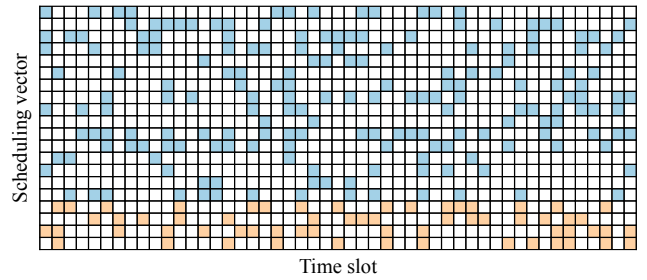


Fig. 5. Device scheduling vectors of the proposed CRL algorithm. $M = 18$. The white blocks indicate $u_{n,t} = 0$, and colored blocks indicate $u_{n,t} = 1$. In each scheduling vector, each black block consumes 1 RB per transmission, and each orange block consumes 5 RBs per transmission.

IV. SIMULATION RESULTS AND DISCUSSION

In our simulation, we consider a wireless network with 20 wireless devices, including 8 thermometers, 8 hygrometers, and 4 positioning sensors. The transmission priority weights \mathbf{w} of the thermometers, hygrometers, and positioning are $\frac{3}{20}, \frac{1}{10}, \frac{1}{20}$, respectively, and the unit cost of RB b for the data transmission at each type of device is 1, 1, 5, respectively. In this setting, scheduling all devices at each time slot consumes $\sum_{n=1}^N b_n = 36$ RBs while only M ($M < 36$) RBs are available for DT synchronization. The proposed algorithm is trained and inferred with combined real-world sensing datasets from Intel Berkeley research lab sensor data [44] and indoor positioning data [45]. Other parameters are listed in Table II. In our simulations, the trained model requires approximately 5 MB of storage and performs each inference with 0.1 ms on an Intel Core i7-13700KF CPU.

The proposed algorithm is compared with three baselines: a) Standard SAC method that schedules devices without the assistance of MTR buffer, b) Polling method that schedules each device by turns, and c) DP based method that schedules each device with fixed time slot intervals solved by DP [37]. The comparison between SAC and the proposed CRL method can justify how the continual learning (CL) mechanism improves convergence performance of the scheduling algorithm

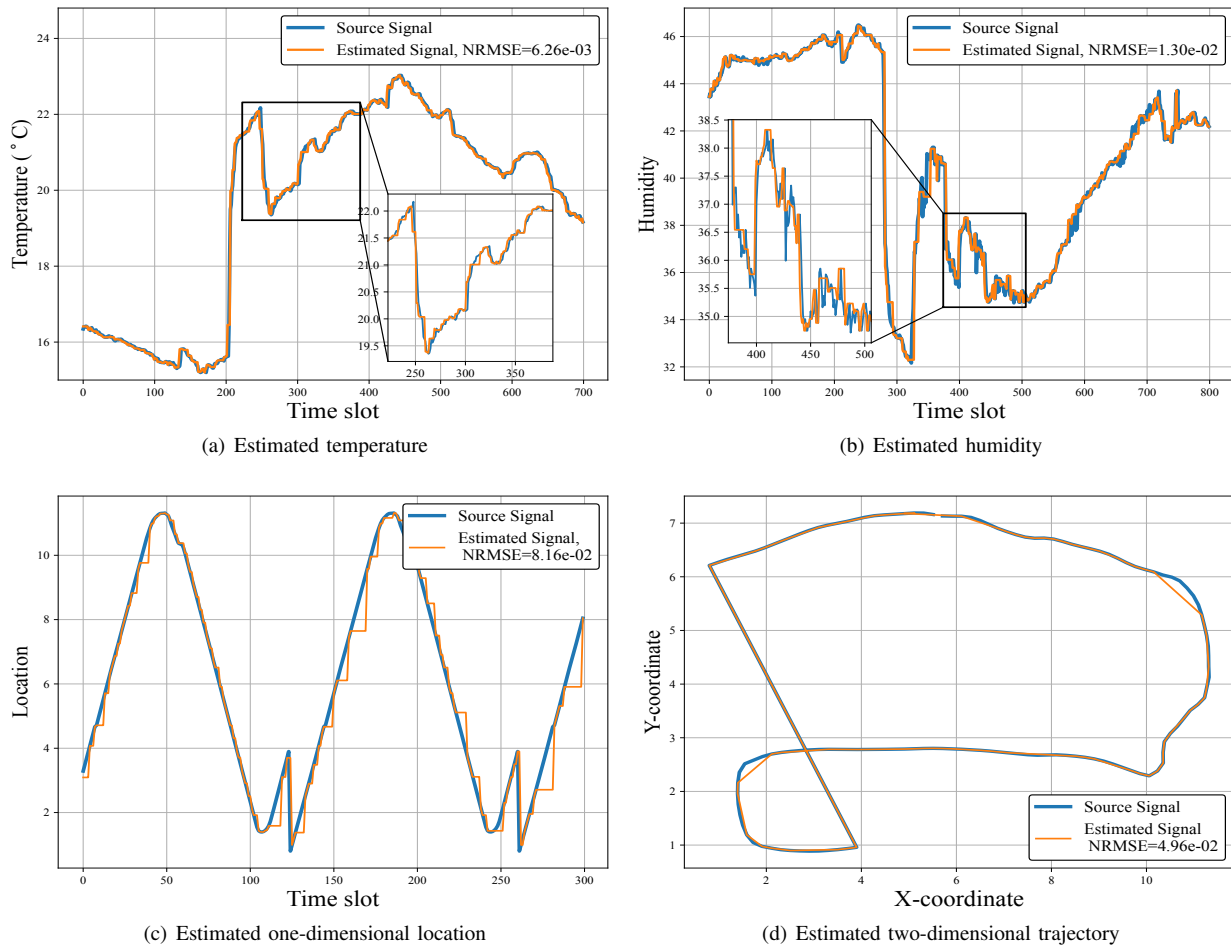


Fig. 6. Estimated virtual state signals and the physical state signals.

within dynamic wireless network capacity. The comparison between the proposed CRL algorithm and the polling method will justify how adaptive scheduling promotes high-accuracy estimation within DT , while the comparison with the DP method demonstrates that the perception of channel conditions in the proposed CRL algorithm further enhances the DT mapping accuracy.

Fig. 4 shows how the proposed MTR-SAC algorithm and standard SAC method converge with changing wireless resources. In the simulation, the number of available RBs M drops abruptly from 30 to 10 at the 200th episode, then increases to 26 at the 400th episode. From Fig. 4 we see that, the rewards of both the methods decrease and increase with the available RB resources as expected. This stems from the fact that the introduced multiplier function can adjust multiplier λ , thereby enabling the agent to adapt to the RB constraint changes. Fig. 4 also shows that the reward of the SAC method fluctuates dramatically after M changes, while that of the MTR-SAC method remain relatively stable. This is because the adopted IRM loss in the MTR scheme can restrain drastic updates of the policy. From Fig. 4, we can also see that, after M changes at the 200th and the 400th episodes, the MTR-SAC method quickly converges while the standard SAC method stays unconverged. This is because the standard SAC method suffers from catastrophic forgetting of old experiences

after M changes, while the MTR buffer scheme and IRM loss refine the common knowledge across different constraints, thereby achieving quick adaptation to new constraints. Fig. 4 also shows that, the proposed MTR-SAC method converges slightly slower than SAC during the initial convergence phase while achieving faster convergence in subsequent phases. This is because the adopted IRM loss in MTR moderates drastic changes in the policy network thus facilitating the learning of common knowledge across diverse constraints. Consequently, the MTR-SAC exhibits slightly slower initial convergence, followed by quicker convergence in dynamics with the learned common knowledge. Thus, the simulation results shown in Fig. 4 can justify the improvement in few shot performance of SAC algorithm with the integrated MTR scheme.

Fig. 5 shows a visualization of device scheduling vectors in a fragment of successive time slots. In Fig. 5 we see that, the proposed CRL algorithm can schedule the on-demand devices with successive time slots, thus guaranteeing the sensed physical state changes are transmitted with enough scheduled RBs. This phenomenon stems from the fact that the adopted mismatch loss functions extract significant state changes, which can be detected by the proposed CRL algorithm. The CRL algorithm then schedules RBs for an appropriate period accordingly. Fig. 5 also shows that each device can be scheduled once within an interval of several time slots,

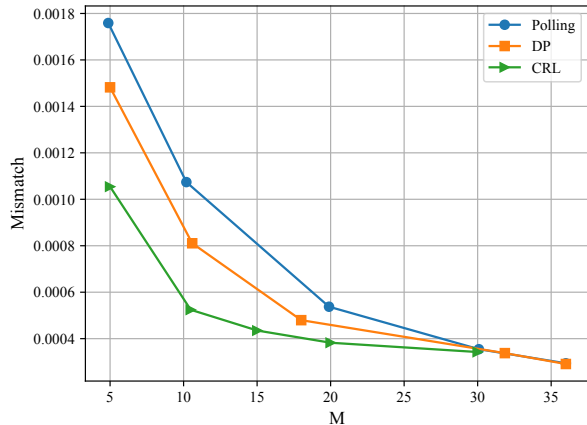


Fig. 7. Weighted mismatch as the number of RBs M increases. In the simulation, all sensing data $X_{n,t}$ is normalized for the convenience of comparison.

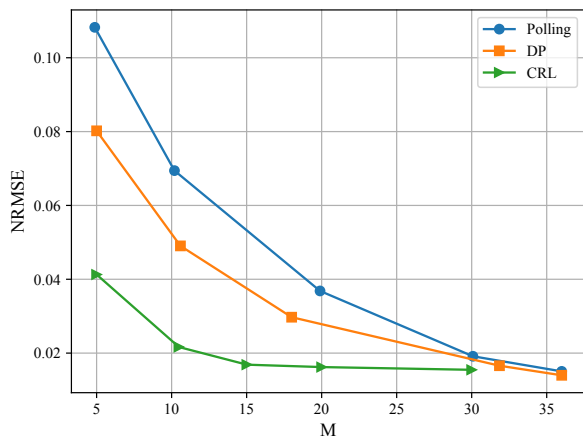


Fig. 8. NRMSE of devices as number of RBs M increases.

thereby maintaining fairness in device scheduling. This is because the CRL algorithm uses action entropy maximization loss in (22) to generate stochastic actions.

Fig. 6 shows 4 examples of the estimated virtual states and the corresponding estimation NRMSE. Notice that the dramatic changes in the estimated signals occur during the synchronization processes within the DT, whereas those in the source signals simply indicate significant changes in the physical system. Then, from Fig. 6 we see that, the proposed CRL algorithm only schedules sensing data transmission for dramatic physical state changes, such that it can follow up with physical system changes with reduced need of data transmission. The reduction is because the proposed mismatch loss functions can capture variations in physical states, identifying the transmissions of inconspicuous state changes as redundant. From Fig. 6, we can also observe that the NRMSE of temperature in Fig. 6(a) is the lowest as the thermometers have the highest transmission priority weight,

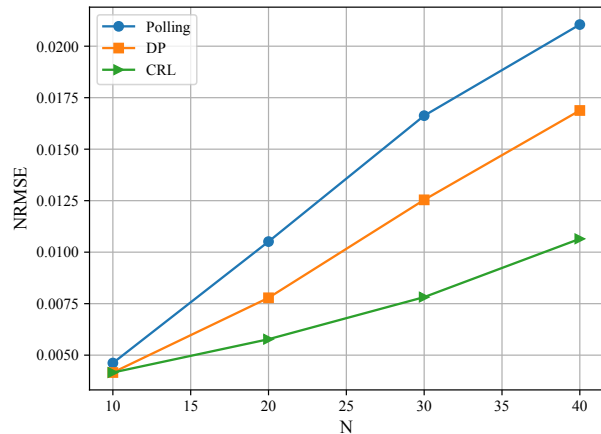


Fig. 9. NRMSE as number of devices N increases, the number of RB constraint is $M = 10$.

while the NRMSE of location in Fig. 6(c) is the highest due to the low transmission priority weight and large RB consumption at positioning sensors. The difference on estimation precision shown in Fig. 6 further validates the proposed CRL algorithm's ability to adapt to different transmission priorities with adjusted device scheduling strategies.

In Fig. 7, we show the changes in the weighted mismatch of all devices with different methods as the number of RBs M increases. Fig. 7 shows that as M increases, the weighted mismatch decreases as expected, and the proposed CRL algorithm obtains a lower weighted mismatch than the baselines. When using 15 RBs, the CRL algorithm can reduce the weighted mismatch by up to 30.58% and 47.63%, respectively, compared to the DP method and polling method. The improvement of the DP method over the polling method lies in the customized scheduling intervals for diverse devices, which capture the characteristics of physical state changes and thereby reduce the mismatch. The improvement of the proposed CRL algorithm over the DP method is attributed to the ability to learn the latest varying trends of physical states and channel conditions, thereby adaptively adjusting the scheduling intervals. Fig. 7 also shows that, when M approaches 36, all the methods exhibit a low mismatch close to 0 because of the abundant RBs. However, as M decreases below 10, the weighted mismatch increases sharply. This is due to the fact that the constrained number of available RBs decrease the scheduled data transmission, thereby affecting the mismatch significantly.

Fig. 8 shows how the averaged NRMSE between virtual states and physical states from all devices changes as the number of RBs M increases. From Fig. 8 we observe that, as M increases, the NRMSE decreases because more RBs can support more frequent sensing data transmission, thus reducing the NRMSE of virtual states. Fig. 8 also shows that, when M is close to 36, all methods have a low NRMSE because the RBs are sufficient to schedule all devices in each time slot. It can also be seen that as M decreases below 10, the NRMSE of all methods increases, with the proposed CRL algorithm exhibiting the slowest increase rate.

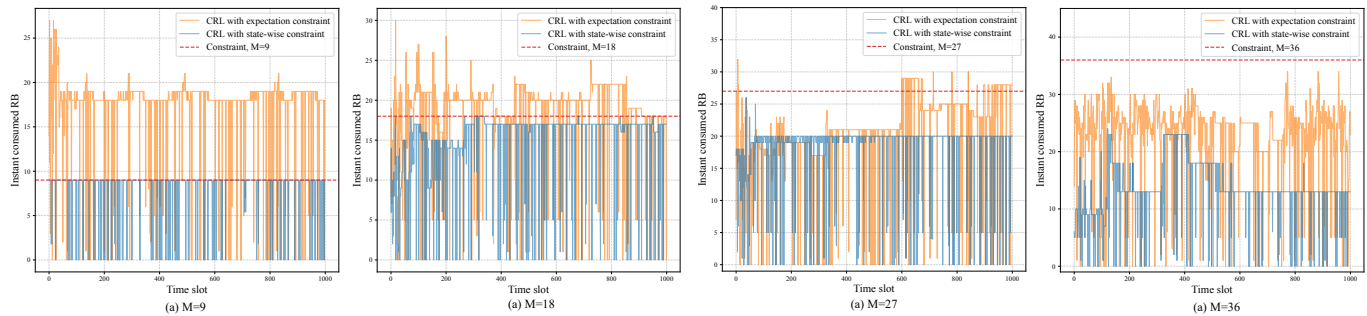


Fig. 10. Instant consumed RBs by the CRL algorithm with different constraints, $M = 9, 18, 27, 36$.

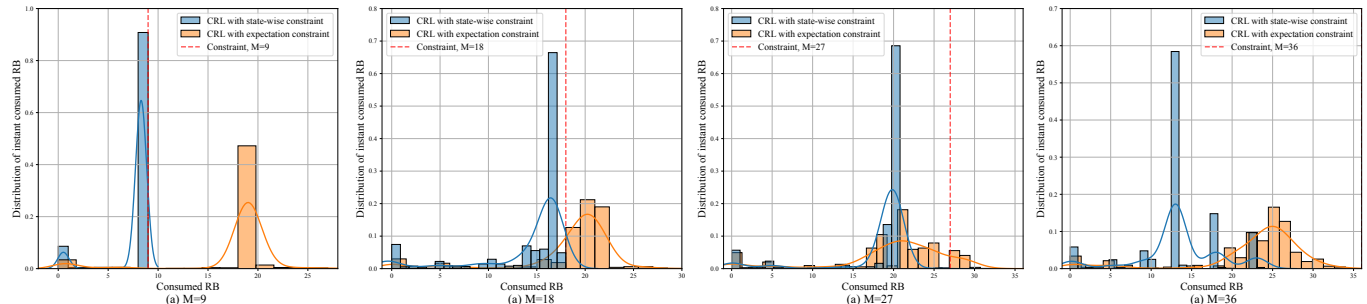


Fig. 11. Distributions of instant consumed RBs, $M = 9, 18, 27, 36$.

This is because that the on-demand synchronization of the frequent and dramatic physical state changes cannot be fully supported by limited number of RBs, leading to an increase of NRMSE at DT. The slower NRMSE increase rate of the CRL method stems from the fact that the proposed CRL algorithm continually learns and predicts the physical dynamics, while the polling and DP methods assume regular changes in the physical state. From Fig. 8 we can also see that, to achieve the same NRMSE of 0.02, the proposed CRL algorithm can reduce the number of consumed RB by up to 55.56% and 61.54% compared to the DP method and the polling method, respectively. And using the same number of RBs with $M = 15$, the proposed CRL algorithm can reduce the NRMSE by up to 55.21% and 68.42% compared to the DP method method and polling method, respectively. The reduction of RB consumptions and NRMSE is because the CRL algorithm learns both the physical state variations and the channel conditions, thus scheduling the devices with effective data. Fig. 7 and Fig. 8 collectively demonstrate that the proposed CRL algorithm offers a more resource-efficient device scheduling solution, particularly in the resource-limited scenarios.

Fig. 9 shows how the average NRMSE of different methods changes as the number of devices N increases. In the simulation, the number of available RB numbers is fixed at $M = 10$, and each device consumes $b_n = 1$ RB per transmission. From Fig. 9 we observe that, when $N = 10$, all methods exhibit low NRMSE due to the sufficient RBs, meanwhile, the polling method has a relatively high NRMSE when $N = 10$ because of the lack of channel condition perception. Fig. 9 also shows that as the number of devices N increases, the NRMSE increases nearly linearly due to the increased RB competition among devices. When $N = 20$, the CRL algorithm can reduce

the NRMSE by 28.84% and 45.09% compared to the DP method and polling method, respectively. From Fig. 9 we can also see that, the CRL algorithm has the slowest increase rate as the number of devices N increase. This is because the CRL algorithm learns both the physical states varying trends and channel condition to support high-density device scheduling with limited RBs. Fig. 9 demonstrates that, compared to the polling and DP methods, the proposed CRL algorithm is more scalable with the enhanced communication resource efficiency in high device density scenarios.

Fig. 10 shows the values of instant consumed RBs by the proposed CRL algorithm with the expectation constraint and the state-wise constraint when $M = 9, 18, 27, 36$. This simulation is conducted to demonstrate the constraint satisfaction performance of solving the state-wise constrained problem. From Fig. 10-(a) and (b) we see that, under resource-scarce conditions ($M = 9$, and 18), the expectation constraint method will tentatively exceed the constraint value M with a significant probability. In contrast, the proposed method, which learns CRL with a state-wise constraint, can significantly guarantee that the instant consumed RBs under the RB capacity constraint. This is because that the state-wise constraint problem formulation imposes stricter limitations on the CRL algorithm, ensuring that RB usage conforms better to practical conditions. Fig. 10-(c) and (d) show that under resource-sufficient conditions ($M = 27$, and 36), the state-wise constraint method uses fewer resources compared to the expectation constraint method, ensuring the RB consumption satisfies the constraint. This is because the cost definition in the proposed CRL method includes a penalty for exceeding the RB capacity, causing the CRL to reduce RB usage thus decreasing the probability of exceeding the capacity constraint. Fig. 10 demonstrates that the proposed method

effectively ensures the satisfaction of the RB constraints.

Fig. 11 shows the distributions of instant consumed RBs in Fig. 10, for $M = 9, 18, 27, 36$. From Fig. 11 we can observe that, the state-wise constraint method results in distributions with smaller means and variances, compared to the expectation constraint method. This phenomenon is attributed to the state-wise constraint compelling the CRL method to use fewer RBs. Furthermore, the IRM mechanism stabilizes the policy output of the CRL method, thus enabling more effective DT synchronization optimization.

V. CONCLUSION

In this paper, we have developed a CRL based adaptive resource allocation scheme to optimize DT synchronization over dynamic wireless networks. To maintain DT synchronization with limited wireless resources, we proposed to selectively schedule devices for data transmission, meanwhile optimize the allocation of RBs over the wireless transmission links. A CMDP problem has been formulated to capture the goal of minimizing long-term mismatch between the physical and virtual systems over device scheduling decisions. To solve the problem, we first transformed the original problem into a dual problem to refine the impacts of RB constraints on device scheduling strategies. Then we proposed a CRL algorithm to solve the dual problem. The CRL algorithm consists of an MTR buffer that stabilizes the SAC policy learning processes across historical experiences, which achieves quick adaptation of device scheduling solutions to the dynamics in physical object states and network capacity. Simulation results have demonstrated that the proposed CRL algorithm is resilient to the changes in wireless network capacity, and shows higher wireless resource efficiency, even in resource-limited, high device density scenarios. The proposed CRL algorithm can reduce NRMSE of the estimated virtual states by up to 55.2%, using the same number of RBs as traditional methods.

APPENDIX

A. Proof of Theorem 1

First, denote $v(\mathbf{Z}) = \frac{1}{N} \mathbf{w}^\top \mathbf{Z}$, the problem $\mathbb{P}2$ can be reformulated by

$$\begin{aligned} \min_{\pi} \quad & \mathbb{E}_{\mathbf{Z} \sim d_0(\mathbf{Z})} v(\mathbf{Z}) \\ \text{s.t.} \quad & d_0(\mathbf{Z}) [V_c(\mathbf{Z}) - M] \leq 0, \forall \mathbf{Z} \in \mathcal{S}_F, \end{aligned} \quad (29)$$

where $d_0(\mathbf{Z})$ is the practical sampled state distribution and \mathcal{S}_F is the feasible region of state.

We consider the constraint of problem (29). The distribution of initial state $d_0(\mathbf{Z})$ has the property of $d_0(\mathbf{Z}) \geq 0$. While the initial feasible state set has the property

$$\mathcal{I} = \{\mathbf{Z} \mid d_0(\mathbf{Z}) > 0\}. \quad (30)$$

Because that for those states not in the possible initial state set, which is $\mathbf{Z} \notin \mathcal{I}$, we have $d_0(\mathbf{Z}) = 0$, according to the definition of possible initial state set. Therefore, the constraint in (29) can be reformulated to

$$V_c(\mathbf{Z}) - M \leq 0, \forall \mathbf{Z} \in \mathcal{I} \cap \mathcal{S}_F, \quad (31)$$

which is equivalent to the constraint in $\mathbb{P}2$

$$V_c(\mathbf{Z}) - M \leq 0, \forall \mathbf{Z} \in \mathcal{I}_F. \quad (32)$$

Since it is infeasible to find a policy which enforces infeasible states to satisfy the constraint, consider that the state distribution $d_0(\mathbf{Z})$ can be sampled from the feasible region \mathcal{S}_F , and an alternative Lagrangian function form of $\mathcal{L}_{\text{stw}}(\mathbf{u}, \lambda)$ in equation (12) can be given by

$$\begin{aligned} \mathcal{L}'_{\text{stw}}(\mathbf{u}, \lambda) &= \mathbb{E}_{\mathbf{Z} \sim d_0(\mathbf{Z})} \{v(\mathbf{Z}) + \lambda(\mathbf{Z}) [V_c(\mathbf{Z}) - M]\} \\ &= \mathbb{E}_{\mathbf{Z} \sim d_0(\mathbf{Z})} \{v(\mathbf{Z})\} + \sum_{\mathbf{Z} \in \mathcal{S}_F} d_0(\mathbf{Z}) \lambda(\mathbf{Z}) [V_c(\mathbf{Z}) - M] \\ &= \mathbb{E}_{\mathbf{Z} \sim d_0(\mathbf{Z})} \{v(\mathbf{Z})\} + \sum_{\mathbf{Z} \in \mathcal{S}_F} \lambda(\mathbf{Z}) \{d_0(\mathbf{Z}) [V_c(\mathbf{Z}) - M]\}, \end{aligned} \quad (33)$$

which is exactly the Lagrangian function of problem (29). Hence, $\mathcal{L}_{0\text{-stw}}(\mathbf{u}, \lambda)$ is equivalent to $\mathcal{L}_{\text{stw}}(\mathbf{u}, \lambda)$. ■

REFERENCES

- [1] Y. Wu, K. Zhang, and Y. Zhang, "Digital twin networks: A survey," *IEEE Internet of Things Journal*, vol. 8, no. 18, pp. 13789–13804, May 2021.
- [2] L. U. Khan, Z. Han, D. Niyato, M. Guizani, and C. S. Hong, "Meta-verse for wireless systems: Vision, enablers, architecture, and future directions," *IEEE Wireless Communications*, pp. 1–7, Aug. 2024.
- [3] L. Hui, M. Wang, L. Zhang, L. Lu, and Y. Cui, "Digital twin for networking: A data-driven performance modeling perspective," *IEEE Network*, vol. 37, no. 3, pp. 202–209, Jun. 2023.
- [4] Y. Zhang, W. Liang, Z. Xu, and X. Jia, "Mobility-aware service provisioning in edge computing via digital twin replica placements," *IEEE Transactions on Mobile Computing*, pp. 1–16, to appear, Apr. 2024.
- [5] M. Li, C. Chen, X. Yang, J. T. Zhou, T. Zhang, and Y. Li, "Toward communication-efficient digital twin via ai-powered transmission and reconstruction," *IEEE Journal on Selected Areas in Communications*, vol. 41, no. 11, pp. 3624–3635, Nov. 2023.
- [6] Y. Ren, S. Guo, B. Cao, and X. Qiu, "End-to-end network sla quality assurance for c-ran: A closed-loop management method based on digital twin network," *IEEE Transactions on Mobile Computing*, vol. 23, no. 5, pp. 4405–4422, Jun. 2024.
- [7] J. Zheng, T. H. Luan, Y. Zhang, R. Li, Y. Hui, L. Gao, and M. Dong, "Data synchronization in vehicular digital twin network: A game theoretic approach," *IEEE Transactions on Wireless Communications*, vol. 22, no. 11, pp. 7635–7647, Mar. 2023.
- [8] P. Jia, X. Wang, and X. Shen, "Digital-twin-enabled intelligent distributed clock synchronization in industrial IoT systems," *IEEE Internet of Things Journal*, vol. 8, no. 6, pp. 4548–4559, Oct. 2021.
- [9] C. Zhou, J. Gao, M. Li, X. Sherman Shen, and W. Zhuang, "Digital twin-empowered network planning for multi-tier computing," *Journal of Communications and Information Networks*, vol. 7, no. 3, pp. 221–238, Sept. 2022.
- [10] L. Zhou, S. Leng, and Q. Wang, "A federated digital twin framework for uavs-based mobile scenarios," *IEEE Transactions on Mobile Computing*, vol. 23, no. 6, pp. 7377–7393, Jun. 2024.
- [11] Y. Xu, H. Zhou, J. Chen, T. Ma, and S. Shen, "Cybertwin assisted wireless asynchronous federated learning mechanism for edge computing," in *Proc. IEEE Global Communications Conference (GLOBECOM)*, Dec. 2021.
- [12] W. Sun, S. Lei, L. Wang, Z. Liu, and Y. Zhang, "Adaptive federated learning and digital twin for industrial internet of things," *IEEE Transactions on Industrial Informatics*, vol. 17, no. 8, pp. 5605–5614, Aug. 2021.
- [13] Y. Dai and Y. Zhang, "Adaptive digital twin for vehicular edge computing and networks," *Journal of Communications and Information Networks*, vol. 7, no. 1, pp. 48–59, Mar. 2022.
- [14] Z. Zhang, Y. Huang, C. Zhang, Q. Zheng, L. Yang, and X. You, "Digital twin-enhanced deep reinforcement learning for resource management in networks slicing," *IEEE Transactions on Communications*, pp. 1–1, May 2024.

- [15] C. Xu, Z. Tang, H. Yu, P. Zeng, and L. Kong, "Digital twin-driven collaborative scheduling for heterogeneous task and edge-end resource via multi-agent deep reinforcement learning," *IEEE Journal on Selected Areas in Communications*, vol. 41, no. 10, pp. 3056–3069, 2023.
- [16] Y. Gong, H. Yao, Z. Xiong, C. L. P. Chen, and D. Niyato, "Blockchain-aided digital twin offloading mechanism in space-air-ground networks," *IEEE Transactions on Mobile Computing*, vol. 24, no. 1, pp. 183–197, 2025.
- [17] Z. Yang, M. Chen, Y. Liu, and Z. Zhang, "A joint communication and computation framework for digital twin over wireless networks," *IEEE Journal of Selected Topics in Signal Processing*, vol. 18, no. 1, pp. 6–17, Dec. 2024.
- [18] Y. Han, D. Niyato, C. Leung, D. I. Kim, K. Zhu, S. Feng, X. Shen, and C. Miao, "A dynamic hierarchical framework for IoT-assisted digital twin synchronization in the metaverse," *IEEE Internet of Things Journal*, vol. 10, no. 1, pp. 268–284, Aug. 2023.
- [19] Z. Yang, M. Chen, Y. Liu, and Z. Zhang, "Optimizing synchronization delay for digital twin over wireless networks," in *IEEE International Conference on Acoustics, Speech and Signal Processing (ICASSP)*, Apr. 2024, pp. 9106–9110.
- [20] J. Tang, J. Nie, J. Bai, J. Xu, S. Li, Y. Zhang, and Y. Yuan, "Uav-assisted digital twin synchronization with tiny machine learning-based semantic communications," *IEEE Internet of Things Journal*, to appear, May, 2024.
- [21] J. Zheng, T. H. Luan, Y. Zhang, R. Li, Y. Hui, L. Gao, and M. Dong, "Data synchronization in vehicular digital twin network: A game theoretic approach," *IEEE Transactions on Wireless Communications*, vol. 22, no. 11, pp. 7635–7647, Mar. 2023.
- [22] M. Seguin, A. Omer, M. Koosha, F. Malandra, and N. Mastrorade, "Deep reinforcement learning for downlink scheduling in 5G and beyond networks: A review," in *2023 IEEE 34th Annual International Symposium on Personal, Indoor and Mobile Radio Communications (PIMRC)*, Sept. 2023, pp. 1–6.
- [23] F. Tang, Y. Zhou, and N. Kato, "Deep reinforcement learning for dynamic uplink/downlink resource allocation in high mobility 5G hetnet," *IEEE Journal on Selected Areas in Communications*, vol. 38, no. 12, pp. 2773–2782, Jun. 2020.
- [24] F. H. Costa Neto, D. C. Araújo, M. P. Mota, T. F. Maciel, and A. L. F. de Almeida, "Uplink power control framework based on reinforcement learning for 5G networks," *IEEE Transactions on Vehicular Technology*, vol. 70, no. 6, pp. 5734–5748, Apr. 2021.
- [25] Q. Liu, L. Tang, T. Wu, and Q. Chen, "Deep reinforcement learning for resource demand prediction and virtual function network migration in digital twin network," *IEEE Internet of Things Journal*, vol. 10, no. 21, pp. 19 102–19 116, Jun. 2023.
- [26] Y. Lu, S. Maharjan, and Y. Zhang, "Adaptive edge association for wireless digital twin networks in 6G," *IEEE Internet of Things Journal*, vol. 8, no. 22, pp. 16 219–16 230, July 2021.
- [27] K. Zhang, J. Cao, and Y. Zhang, "Adaptive digital twin and multi-agent deep reinforcement learning for vehicular edge computing and networks," *IEEE Transactions on Industrial Informatics*, vol. 18, no. 2, pp. 1405–1413, Feb. 2022.
- [28] X. Tang, X. Li, R. Yu, Y. Wu, J. Ye, F. Tang, and Q. Chen, "Digital-twin-assisted task assignment in multi-uav systems: A deep reinforcement learning approach," *IEEE Internet of Things Journal*, vol. 10, no. 17, pp. 15 362–15 375, Mar. 2023.
- [29] 3rd Generation Partnership Project (3GPP), "3GPP TS 23.501: System Architecture for the 5G System (5GS)," <https://www.3gpp.org/dynareport/23501.htm>, Dec. 2017.
- [30] Y. Xi, A. Burr, J. Wei, and D. Grace, "A general upper bound to evaluate packet error rate over quasi-static fading channels," *IEEE Transactions on Wireless Communications*, vol. 10, no. 5, pp. 1373–1377, May 2011.
- [31] P. Reichl, S. Egger, R. Schatz, and A. D'Alconzo, "The logarithmic nature of qoe and the role of the weber-fechner law in QoE assessment," in *International Conference on Communications*, Cape Town, South Africa, May 2010.
- [32] X. Xu, A. Peng, X. Hong, Y. Zhang, and X.-P. Zhang, "Multistate constraint multipath-assisted positioning and mismatch alleviation," *IEEE Internet of Things Journal*, vol. 11, no. 7, pp. 11 271–11 286, Nov. 2024.
- [33] E. Altman, *Constrained Markov decision processes*. Routledge, Dec. 2021.
- [34] N. Cheng, X. Wang, Z. Li, Z. Yin, T. Luan, and X. S. Shen, "Toward enhanced reinforcement learning-based resource management via digital twin: Opportunities, applications, and challenges," *IEEE Network*, vol. 1, no. 1, pp. 1–7, Aug. 2024.
- [35] C. Kaplanis, C. Clopath, and M. Shanahan, "Continual reinforcement learning with multi-timescale replay," *arXiv:2004.07530*, Apr. 2020.
- [36] H. Ma, Y. Guan, S. E. Li, X. Zhang, S. Zheng, and J. Chen, "Feasible actor-critic: Constrained reinforcement learning for ensuring statewise safety," *arXiv:2105.10682*, May 2021.
- [37] A. Maatouk, M. Assaad, and A. Ephremides, "The age of incorrect information: an enabler of semantics-empowered communication," *IEEE Transactions on Wireless Communications*, to appear, 2022.
- [38] D. Ding, C.-Y. Wei, K. Zhang, and A. Ribeiro, "Last-iterate convergent policy gradient primal-dual methods for constrained MDPs," in *Advances in Neural Information Processing Systems (NeurIPS)*, vol. 36. Curran Associates, Inc., Dec. 2023.
- [39] T. Haarnoja, A. Zhou, P. Abbeel, and S. Levine, "Soft actor-critic: Off-policy maximum entropy deep reinforcement learning with a stochastic actor," in *Proc. Int. Conf. on Mach. Learning (ICML)*, vol. 80, Jul. 2018.
- [40] T. Haarnoja, A. Zhou, K. Hartikainen, G. Tucker, S. Ha, J. Tan, V. Kung, H. Zhu, A. Gupta, P. Abbeel *et al.*, "Soft actor-critic algorithms and applications," *arXiv:1812.05905*, Dec. 2018.
- [41] M. Arjovsky, L. Bottou, I. Gulrajani, and D. Lopez-Paz, "Invariant risk minimization," *arXiv:1907.02893*, Mar. 2020.
- [42] H. Tong, S. Wang, Z. Yang, J. Zhao, M. Bennis, and C. Yin, "Semantic-aware remote state estimation in digital twin with minimizing age of incorrect information," in *IEEE Global Communications Conference (Globecom)*, Kuala Lumpur, Malaysia, Dec. 2023.
- [43] H. Tong, Z. Yang, S. Wang, Y. Hu, W. Saad, and C. Yin, "Federated learning based audio semantic communication over wireless networks," in *Proc. IEEE Global Communications Conference (GLOBECOM)*, Madrid, Spain, Dec. 2021.
- [44] P. Bodik, W. Hong, C. Guestrin, S. Madden, M. Paskin, and R. Thibaux, "Intel berkeley research lab sensor data," Downloaded from <http://db.csail.mit.edu/labdata/labdata.html>, Jun. 2004.
- [45] S. Sun, "Indoor received signal strength data generated from ray-tracing," Dec. 2020. [Online]. Available: <https://dx.doi.org/10.21227/r9n4-xz17>